

Models for Accretion Disk Fluctuations through Self-Organized Criticality Including Relativistic Effects

Ying XIONG, Paul J. WIITA and Gang BAO¹

Department of Physics and Astronomy, Georgia State University,

University Plaza, Atlanta, Georgia 30303, USA

¹*current address: CIS Department, Columbia University, 525 W. 120th St., New York, New York 10027, USA*

E-mail(PJW): wiita@chara.gsu.edu

(Received 2000 June 2; accepted 2000 August 4)

Abstract

The possibility that some of the observed X-ray and optical variability in active galactic nuclei and galactic black hole candidates is produced in accretion disks through the development of a self-organized critical state is reconsidered. New simulations, including more complete calculations of relativistic effects, do show that this model can produce light-curves and power-spectra for the variability which agree with the range observed in optical and X-ray studies of AGN and X-ray binaries. However, the universality of complete self-organized criticality is not quite achieved. This is mainly because the character of the variations depend quite substantially on the extent of the unstable disk region. If it extends close to the innermost stable orbit then a physical scale is introduced and the scale-free character of self-organized criticality is vitiated. Significant dependence of the power spectrum density slope on the type of diffusion within the disk and a weaker dependence on the amount of differential rotation are noted. When general relativistic effects are incorporated in the models, additional substantial differences are produced if the disk is viewed from directions far from the accretion disk axis.

Key words: Accretion, accretion disks — Black holes — Galaxies: active — Hydrodynamics — Relativity — X-rays: binaries

1. Introduction

Structures within accretion disks can be observed indirectly through the luminosity variations they engender. Several hydrodynamical processes could produce such irregularities. Vortices (e.g. Abramowicz et al. 1992; Bracco et al. 1999) and shocks induced by companion objects (e.g. Sawada, Matsuda, & Hachisu 1986; Chakrabarti & Wiita 1993) are among the physical mechanisms that can yield significant long-lived (multi-orbit) perturbations on disks.

Any such quasi-coherent structures can produce “bright spots” on the disk surfaces. These regions of excess emission, when coupled with the disk’s differential rotation and gravitational lensing of photons passing close to the central black hole, can reproduce many aspects of the variations seen in galactic black hole-candidates and active galactic nuclei (AGN). The X-ray light curves and power spectra (Abramowicz et al. 1989, 1991; Zhang & Bao 1991), and optical/UV light curves and power spectra (Wiita et al. 1991; Mangalam & Wiita 1993) can both be understood within this bright spot model. The anti-correlation between X-ray variability and luminosity in AGN, confirmed by Lawrence & Papadakis (1993), can also naturally be explained using this model (Bao & Abramowicz 1996). It has also been demonstrated that the surprisingly strong coherence in the temporal variability seen between different X-ray energies for galactic black hole binaries (Vaughn & Nowak 1997) is also capable of being understood within the bright spot framework (Abramowicz et al. 1997). This scenario also predicts energy dependent polarization variations in the X-ray bands (Bao, Wiita & Hadrava 1996; Bao et al. 1997) which could be detected by future X-ray satellites with polarimetric capabilities. In addition, changes in the X-ray spectra of Seyfert galaxies can be understood in terms of varying amounts of reprocessing and reflection involving such irregular accretion disks (Bao, Wiita & Hadrava 1998; Bao & Wiita 1999).

If accretion disks exhibit self-organized criticality (SOC), as first suggested by Mineshige, Ouchi & Nishimori (1994a), then another way to directly produce temporally extended quasi-coherent structures is available. The SOC concept arose from the realization that a huge range of physical systems display power-law or scale-invariant correlations over decades in time or space. “Flicker noise” or “1/f noise” is seen in a wide variety of systems, ranging from stock market prices, through the height of the Nile river, to quasar light curves (e.g. Press 1978). Bak, Tang & Wiesenfeld (1987, 1988) showed extended systems with many metastable states can naturally evolve into a critical state with no fundamental length- or time-scales.

In § 2 we briefly summarize characteristics of the SOC state, and then we mention some suggested astrophysical

applications. In §3 we discuss earlier efforts to show how this might work in accretion disks. In §4 we display and discuss additional computations of modified SOC models for disks which display a goodly range of light curves and variability power spectra. Some preliminary results (without, however, including relativistic effects) were presented earlier (Wiita & Xiong 1999; hereafter, WX). We find that the slopes of the power spectral density are quite sensitive to the extent of the region that is unstable, so that these accretion disk models do not exhibit self-organized criticality in the strictest sense. Our conclusions are given in §5.

2. Characteristics of Self-Organized Criticality

2.1. *The sandpile model*

A sandpile was the first toy model for self-organized criticality, and the original papers by Bak et al. (1987, 1988) performed numerical simulations relevant to this situation, transformed into a cellular automata problem. One drops grains of sand randomly onto a pile until it builds up to a critical slope or “angle of repose”. Once the pile is at SOC, the addition of a single extra grain of sand anywhere causes the local slope to be too steep. This leads to a small avalanche which readjusts the local slope to just below critical. But now the moved sand will steepen the region of the pile just below it, perhaps making that region, in turn, too steep. Avalanches continue until the local slope everywhere adjusts to be at, or just below, the critical value.

The system becomes stationary when perturbations can just propagate the length of the system, and a full-fledged SOC state of any physical system has the following characteristics: a distribution of minimally stable regions of all sizes; small perturbations can yield “avalanches” of all sizes; the lack of any characteristic length scale produces a featureless power-law spectrum of avalanche sizes; the critical state is insensitive to initial conditions.

Unsurprisingly, different physical systems have different power-law indices for the relation between the number of events (avalanches) that occur with different sizes or strengths. These indices depend on (Bak et al. 1988; O’Brien et al. 1991): the number of spatial dimensions; the symmetry of the system; and the attractor of the dynamics of the system. For two-dimensional sandpile models, Bak et al. (1988) found the power spectral density for the Fourier transform of the time-series to be $S(f) \propto f^{-1.57}$; for three-dimensional models they obtained $S(f) \propto f^{-1.08}$.

2.2. Application to solar flares

The first astronomical application of this concept was the proposal by Lu & Hamilton (1991) that the solar coronal magnetic field is in a SOC state. They noted that observations of hard X-ray bursts in solar flares have a distribution that is a power-law in peak photon flux with logarithmic slope 1.8 over up to five decades: $N(P) \propto P^{-1.8}$ (e.g. Dennis 1985).

The Lu & Hamilton model assumes that the flares are avalanches of smaller magnetic reconnection events and that all flares arise from the same physical process. A lattice picture in three dimensions assumes the local field gradient is destroyed by reconnection when the local magnetic gradient is too large, as argued by Parker (1988). The magnetic gradient vector of a lattice point which exceeds this limit is eliminated at that particular location, but the gradient is shared with neighboring lattice points. In order for this model to work, changes in magnetic field must have a directionality (i.e., photospheric motions should on average increase B in a particular direction, a not unreasonable assumption over substantial areas).

The results of their simulations can be summarized as follows: energy release goes as $N(E) \propto E^{-1.4}$; peak flux goes as $N(P) \propto P^{-1.8}$ (as observed). Lu & Hamilton (1991) argue that these power-law indices are rather insensitive to the critical field gradient. While this picture is not exactly well motivated physically, it does incorporate some viable assumptions and does produce a way to understand an otherwise unexplained relation between the size and frequency of solar flares. Additional physical conditions as well as implications of this idea have been explored by Lu (1995).

2.3. Application to Gamma-Ray Bursts

Similar “avalanches” or “chain reactions” may play a role in understanding details of gamma-ray bursts (Stern & Svensson 1996). While the time profiles of γ -ray bursts (GRBs) show a very wide range of behaviors, there are several statistical properties that have specific mathematical structures. The average peak-aligned profile and the autocorrelation function show stretched exponential behaviors. This could imply that the wide range of GRB characteristics could arise from different random realizations of a simple stochastic process which is scale invariant in time.

The Stern & Svensson (1996) model is based upon a pulse avalanche, where a trigger event induces many additional flares by setting off a “chain reaction” in a near-critical regime. Such a basic picture was shown to fit both the

diversity of GRB time-profiles and important average statistical properties of GRBs, such as their third-moment, their autocorrelation function and their duration distribution function. Similarly to Lu & Hamilton (1991), Stern & Svensson (1996) suggest that magnetic reconnection in a turbulent medium is a plausible underlying mechanism, one that can fit within exploding fireball or relativistic jet models for GRBs.

3. SOC and Accretion Disks

The first proposal that accretion disks around black holes could be in an SOC state was made by Mineshige, Ouchi & Nishimori (1994a). This was an attempt to produce the steeper than $\sim 1/f$ fluctuations seen in X-ray power-spectrum densities (PSD) for BH candidates such as Cyg X-1 (e.g. Miyamoto et al. 1993). This could provide physical connections between bright spots (or determine the size thereof) and thereby engender coherent structures for interesting lengths of time. Our work in this paper is essentially an extension and modification of this pioneering effort, so we shall describe their approach in moderate detail. An extensive review and discussion of other aspects of this approach has been given recently by Mineshige & Negoro (1999).

The outer disk is assumed to be smooth enough so as to not produce any variability; however, the inner disk is subject to some, not yet physically constrained, instability. (Mineshige et al. suggest this instability could be related to flares in the corona, presumed to lie above and below the disk, in analogy with Lu & Hamilton's solar corona picture.) The unstable inner disk is divided into zones (i, j) characterized by radial (r_i) and azimuthal (ϕ_j) coordinates and taken to be geometrically thin. To model ordinary viscous accretion, the outer disk feeds a mass particle, m , to a zone in the outermost ring of the inner disk, r_1 , with random ϕ . In lieu of more developed physics, Mineshige et al. (1994a) assume $M_{\text{crit},i} \propto r$. If the mass contained in the $(i, j)^{\text{th}}$ zone, $M_{i,j} > M_{\text{crit},i}$, they then assume enough mass is dumped from zone (i, j) to bring $M_{i,j} \leq M_{\text{crit},i}$. This excreted mass is taken to spread to the three nearest zones one ring interior to the destabilized zone (for simulations corresponding to rigid rotation) or to three trailing interior zones (as a simple way of mimicking differential rotation).

After the mass has been dumped from an overloaded zone into others closer to the central mass, one must test those adjacent interior zones for $M_{i+1,(j-1,j,j+1)} > M_{\text{crit},i+1}$ (these choices for the second subscript pertain to rigid rotation). If this condition is fulfilled, one continues the avalanche by dumping mass into next ring inwards. They

reasonably estimate the luminosity for each dumped m by:

$$L_x \simeq (GM_{\text{BH}}m) \left(\frac{1}{r_f} - \frac{1}{r_i} \right), \quad (1)$$

where M_{BH} is the mass of the central black hole, and r_i and r_f are the initial and final radii experienced by that particular mass unit during that particular flow inwards. Then one sums up for the energy released by all avalanching masses. Finally, one reinjects mass at the outer edge of the inner disk and repeats the above procedures. For their canonical disk model, Mineshige et al. (1994a) discover approximate scalings where the number of events vary with their energy as $N(E) \propto E^{-1.35}$, the lifetime distribution varies as $N(\tau) \propto \tau^{-1.7}$, and the PSD follows $S(f) \propto f^{-1.8}$. They showed these power-law indices, or slopes, to be nearly independent of the amount of differential rotation artificially implemented in their simulations.

This type of scenario was also proposed by Yonehara, Mineshige & Welsh (1997) as a way to explain the PSD of optical and ultraviolet fluctuations in cataclysmic variables.

3.1. Diffusion Plus Avalanches in Disks

The above scenario was modified by Mineshige, Takeuchi & Nishimori (1994b), who included gradual mass inflow in every timestep, even if all zones were stable, with $M_{i,j} < M_{\text{crit},i}$. By doing so Mineshige et al. (1994b) were able to model continuous accretion through viscosity in the disk, even in the absence of substantial mass flow (and energy release) produced through instabilities. In their new standard model they transferred $3m$ if a zone is unstable (as before) and also $0.01m$ from one randomly chosen cell in each ring during each fundamental timestep.

The key result was that the PSD index β for $S(f) \propto f^{-\beta}$ was reduced from ~ 1.8 to ~ 1.6 . They note that this is in better agreement with AGN (e.g. Lawrence & Papadakis 1993) and galactic BH candidate data (e.g. Miyamoto et al. 1993). Raising the diffusion rate substantially lowers β somewhat further. Other results from these models are that diffusion produces more small-scale avalanches in the inner regions, and decreases the chance for bigger flares. Small shots (energy releases) usually appear randomly in time since the mass is deposited into the outer ring at random points. On the other hand, big shots could have a non-random temporal distribution because a big event drains many cells below their critical values and therefore a longer time is needed to build back up to the critical state. Careful studies of the temporal distribution of flares of various sizes could therefore, in principle, provide a test of this SOC-type model. An exponential distribution of peak intensities arises from this model and provides a better fit to some of the data (Takeuchi, Mineshige & Negoro 1995).

3.2. *Extrinsic, relativistic modifications*

Preliminary and quite approximate considerations of general relativistic effects, primarily Doppler boosts and gravitational light bending, were also shown to lower β (Abramowicz & Bao 1994). This work combined the basic idea of the bright-spot model (§ 1) with the SOC concept, but involved significant analytical approximations. The extent to which these extrinsic effects modify the PSD index is a strong function of the viewing angle, i , to the normal to the disk plane in this approximation. Larger values of i were found to produce shallower slopes, with β reduced to ~ 1.4 for $i = 80^\circ$ from ~ 1.8 for $i = 0^\circ$ (Abramowicz & Bao 1994).

3.3. *Application to Advection Dominated Accretion Flows*

This model was further modified by Takeuchi & Mineshige (1997) to incorporate key features of the advection dominated accretion flows, which were first suggested by Ichimaru (1977) and since invoked by many others (e.g. Chen et al. 1995). They pointed out that such flows could provide an even better substrate in terms of satisfying several details of observations of galactic BH candidates. The basic nature of the X-ray shot was argued to be well fit by a disturbance propagating inward through an advection dominated disk (Manmoto et al. 1996) and Takeuchi & Mineshige (1997) built upon this concept. They considered various values of the critical radius at which the surface density became too high, and showed, within the framework of a time-dependent but one-dimensional calculation, that flatter PSDs were obtained for larger values of this critical radius.

4. **Extended Models for SOC in Accretion Disks**

Our new efforts have involved making changes to various parameters for models similar to those suggested by Mineshige et al. (1994a,b) to see if the light curves and power spectra for the fluctuations were actually as independent of initial and boundary conditions as they suggested, particularly when general relativistic effects were included. We must stress that all of our work to date has been restricted to non-rotating black holes. We examined models with different values of the:

- inner and outer radii of the unstable inner portion of the disk;
- viewing angle;
- amount of mass dumped when a cell exceeded the stability limit;

- amount of differential rotation in the location of the zones where the mass is dumped;
- diffusion to sideways and outward as well as inward zones;
- initial deviations from critical density;
- accretion rate.

4.1. Results excluding relativistic effects

Some preliminary results, not including proper relativistic effects and therefore only able to consider face-on views of the disks, were given in WX. As a first step towards inclusion of relativistic effects, we have also modified the gravitational potential from the Newtonian, with $\Phi \propto r^{-1}$, to the pseudo-Newtonian type, $\Phi \propto (r - 2)^{-1}$; the latter “Paczynski – Wiita potential” quite accurately reproduces many of the leading effects of the Schwarzschild geometry (Paczynski & Wiita 1980; Artimova, Björnsson & Novikov 1996). With the above expressions we begin the use of notation where distances are given in units of $r_g = GM_{BH}/c^2$. Then the energy released is,

$$L_x \simeq (GM_{BH}m) \left(\frac{1}{(r_f - 2)} - \frac{1}{(r_i - 2)} \right). \quad (2)$$

We begin by summarizing our first simulations, which did not include relativistic effects (these were discussed in more detail in WX). These early simulations used the standard model of Mineshige et al. (1994a), with 64 rings of unit radius extending inward from $r_1 = 100$ and with the individual zones starting just slightly below critical densities; given those parameters we do indeed reproduce a quasi-power law PSD with slope $\beta \approx 1.8$. We then considered simulations where the radial extent of each ring was modified to produce equal intervals in the logarithm between specified inner and outer radii, and found that for the situation considered by Mineshige et al. (1994a), differences between uniform and logarithmic gridding were negligible, so we have adopted the logarithmic scaling in our work. This allows for smaller unit regions of emission closer to the central BH, which is more realistic as larger gradients of the gravitational field exist in regions close to the black hole; it also better tracks the increase in density and magnetic field energy expected in inner disk regions. In all of our work, the amount of mass dumped from each zone that is triggered by being pushed over its critical value is assumed to be constant, and is denoted by m_d , despite the varying sizes of the zones.

These PSD slopes depend only very weakly upon most of the parameters needed to characterize the simple model. Unsurprisingly, the early stages of the light curves are very sensitive to the initial deviations from the

critical density. Only very small fluctuations are seen at early times if the dumped mass satisfies the inequality, $m_d/3 < M_{\text{crit}} - M_{\text{init}} \equiv \Delta M$; however, the disks eventually approach the critical values in most zones, and the later portions of the light-curves appear similar to each other. The stable portions of the PSDs (those pertaining to higher frequencies) have very similar slopes even if there is a substantial delay before the critical state is reached throughout the disk. Thus we do not display here results involving modifications to the initial deviation from critical density.

Low values of the accretion rate tend to yield larger numbers of flares of specific energies, since, at early times, only single mass dumps or small multiples of these fixed mass dumps (and hence energy production) are induced. In such cases the light curves can retain a banded (or “quantized”) appearance for significant times (see Fig. 3 of WX); nonetheless, values of β are quite independent of \dot{M} , once “avalanches” of wider ranges occur, and an at least quasi-SOC situation is established.

In our non-relativistic simulations we also found the following effects, which we will discuss more completely in §4.2, since they were also considered using our relativistic code. In modeling differential rotation, both the constant extra zone shifts considered by Mineshige et al. (1994a) and variable zone shifts, which better approximate some effects of the actual Keplerian rotation curves, were considered. But in all cases, we found only small changes in light curves or slopes of the PSDs ($\Delta\beta < 0.04$), in agreement with Mineshige et al. (1994a). Further, in agreement with Mineshige et al. (1994b) we found more dependence of the results on the nature of the diffusion. They showed that if there is extra diffusion inward, then the slope of the PSD becomes shallower. This additional diffusion is a reasonable approximation to standard viscosity in disks, which transports matter inwards and angular momentum outwards. We also performed simulations which allow for a more general diffusion of energy, which might be more realistic if actual magnetic reconnection events do indeed provide the physical trigger. To allow for propagation of a disturbance partially sideways and back outwards as well as inwards (which was still presumed to dominate) we also considered cases where the mass outflow from an unstable zone would go 1/5 to each of three interior zones (thus 60% inwards), 1/8 to each of the two neighboring zones in the same ring (25% sideways) and 1/20 to each of the three exterior zones (15% outwards). We find that if the triggering zone can send some matter back outwards and sideways, then the PSD slope can become steeper by up to $\Delta\beta \approx 0.15$ –0.25 in the non-relativistic approximation (cf. Fig. 4 of WX).

For the non-relativistic simulations we found a substantial sensitivity of the power spectrum density index β to the location of the disk's inner radius (r_N) with respect to its outer radius (r_1). Even without including diffusion, $1.1 < \beta < 1.8$, was found, with the shallowest slopes corresponding to $r_N \approx 6$, i.e., at the innermost stable orbit for a non-rotating black hole, when the outer radius is fixed at $r_1 = 200$. Some modest changes are induced by changing the energy released in Eq. (1) from a pure Newtonian, and nominally scale free, r^{-1} dependence, to the pseudo-Newtonian, $(r - 2)^{-1}$, dependence of Eq. (2). In cases where the inner radius was set at $r_N = 6$, so this effect would be maximized, we found the slope to flatten by $\Delta\beta \approx 0.1$.

4.2. Results of Relativistic Simulations

In that most accretion disks will be viewed at some angle other than face-on ($i = 0^\circ$), it is important to consider what effect alternate viewing angles could produce on the observed light curves and PSDs. As mentioned in §3.2, Abramowicz & Bao (1994) incorporated an approximate treatment of such effects and noted that significant flattening of the PSD slope could be expected. In our current work, we have used a more thorough treatment of relativistic effects on the propagation of energy emitted in the vicinity of a Schwarzschild black hole.

Our calculations retain the basic scenario of Mineshige et al. (1994a) as modified by WX; the basic procedure is discussed above and described in more detail in Mineshige et al. (1994a, b) and Mineshige & Negoro (1999). But the results presented here incorporate both the pseudo-Newtonian potential to describe energy release (approximate, but reasonable, given the phenomenological nature of the instability model) as well as full general relativistic (GR) effects on the propagation of the emerging radiation. Note that the light curves presented below exaggerate the magnitude of the fluctuations in that no effectively quiescent underlying disk emission has been included. However, the preemptive subtraction of this mean level does not affect the PSDs.

These GR effects on propagation consist of light-travel time differences, gravitational redshifts, Doppler boosting, and near-field gravitational lensing, and are computed using the efficient techniques described in Bao, Hadrava & Ostgaard (1994) and Bao et al. (1997); we refer the reader to these works and do not repeat the details of these techniques here. For a given location of an element (r, ϕ) , and the viewing angle of the observer (i), we can easily integrate the general relativistic effects on photons emitted by the element into the observed light intensity. We note that these techniques have been generalized to predict the nature of polarization variability from unsteady accretion disks (Bao et al. 1996, 1997) and have been successfully applied to emission from radio jets (Bao & Wiita 1997) and

to the X-ray variability from Seyfert galaxies (Bao, Wiita & Hadrava 1998; Bao & Wiita 1999).

The radiation is assumed to emerge uniformly from each grid zone. These zones have an essentially Keplerian azimuthal velocity taken to vary as (Paczynski & Wiita 1980)

$$v_\phi(r) \propto \left(\frac{GM_{BH}}{r}\right)^{1/2} \left(\frac{r}{r-2}\right), \quad (3)$$

and are normalized to have $0.5c$ at $r = 6$, which is exact for standard thin accretion disks (e.g. Shakura & Sunyaev 1973). For such thin disks the radial component of the flow, $v_r \ll v_\phi$, except for very close to $r = 6$, and thus v_r can be neglected in our calculations. The lifetime of the emission from each triggered zone is taken to be 8 times the local orbital period; while somewhat arbitrary, this assumption allows a full range of variations to build up. The simulations are run for extended periods, with the results reported here based on taking either 4×10^5 or 1×10^6 timesteps. Each timestep corresponds to $1/64$ of the orbital period at the inner edge of the unstable disk region, so that thousands of orbits (even at the outer edge of the unstable disk region) are considered. Thus, if an SOC state were to be established, these simulations are lengthy enough to discern it (e.g. Mineshige & Negoro 1999). Aside from our not considering Kerr geometries, one other geometrical limitation of these models must be stressed: the accretion disk is assumed to be completely thin and flat. The PSDs are determined from the “observed” light curves, i.e., after GR effects on propagation are included, using *Mathematica*. The slopes of these PSDs, β are computed from the dominant region of the PSD; on the scale-free PSDs presented below, this region is defined as extending over 1.6 decades in frequency, from 50 to 2048.

Table 1 summarizes the parameters of the 43 different simulations we have performed and analyzed in this current work. All of these include the relativistic effects discussed above. The column headings identify the Case, give the inner ($r_{in} \equiv r_N$) and outer ($r_{out} \equiv r_1$) radii, the viewing angle, the type of rotational prescription considered, the type of diffusion prescription considered, and the amount of mass dumped when a zone goes unstable; the summary output parameter is the slope of the PSD in the region at high enough frequency that an approximate power-law is established. In several cases, multiple realizations of the same parameters have been averaged; however, since the computed PSD slopes, β , never varied by more than 0.02 between such different realizations, in general only single realizations of these simulations are used to produce the values of β quoted in Table 1.

Cases 1–9 illustrate the situation for disks where only a very limited inner region, from $r_N = 6$ to $r_1 = 19$, is unstable. Such a situation is expected in many standard thin accretion disk models where radiation pressure

dominates the innermost portions (e.g. Lightman & Eardley 1974). We also note that transonic accretion flows yield shocks at comparable radii, and the flow within these regions is more unstable (e.g. Chakrabarti 1996). The differences between the individual Cases in this first group involve changing the viewing angle from face-on ($i = 0^\circ$), where focusing and light-travel delays due to GR are negligible, though red-shifts and resulting reductions in observed power from the innermost regions still play a small role, to nearly along the disk ($i = 85^\circ$), where gravitational focusing can strongly amplify energy releases emitted on the opposite side of the disk from the observer (e.g. Bao et al. 1998). A light-curve and PSD for Case 2 are displayed in Fig. 1. The entries in Table 1 for Cases 1–6 show that the PSD flattens as the inclination angle rises from 0° up through 60° , with a total change of $\Delta\beta \simeq 0.35$, in rough accord with the more approximate calculations of Abramowicz & Bao (1994). As the inclination rises, the effects of Doppler shifts act to enhance effects of energy avalanches extending close to the BH since the velocities there are higher. This raises the power at higher frequencies with respect to those at lower frequencies, thereby flattening the PSD. As the viewing angle increases still further, near-field gravitational lensing becomes more important and the PSD steepens again for $i > 70^\circ$. This effect was not found in the more approximate treatment of Abramowicz & Bao (1994).

In the subsequent sets of simulations we explore situations where larger regions of the disk are taken to be unstable. For Cases 10–18 the inner boundary remains at the last stable circular orbit, but the outer radius is extended to $32(GM_{BH}/c^2)$. Cases 19–27 again have the same inner boundary, but the outer boundary is taken to go all the way out to 100. The key result of these simulations is that, by including larger regions of instability, the slope of the PSD flattens considerably. Figure 2 gives a light curve and PSD for Case 11, and Fig. 3 is for Case 20; these have the same inclination (and all other properties) as did Case 2, illustrated in Fig. 1. The fundamental trend of producing substantially flatter PSDs from larger unstable regions is very clear, with $\Delta\beta \sim 0.10 - 0.25$ between $R_1 = 19$ and $R_1 = 32$ (the extent of the change in slope varies with viewing angle), and $\Delta\beta \sim 0.7 - 0.8$ between $R_1 = 19$ and $R_1 = 100$. Trends with viewing angles, for fixed boundary radii, are similar to those seen in Cases 1–9: as i rises from 0° to higher angles (70° for $R_1 = 32$; 80° for $R_1 = 100$) the value of β drops by ~ 0.25 from the value for face-on observations, demonstrating how the Doppler boosts become more important. But, at the very highest angles, the near-field lensing plays a dominant role, partially reversing the flattening. Unsurprisingly, the greater the outward extent of the unstable region, the lower the relative importance of the latter effect, and the “turn-around” in the slope of the PSD begins at higher angles and is less pronounced. Figure 4 shows some of this particular variation,

displaying Case 13, which has a higher inclination, but is otherwise identical to Case 11 (Fig. 2).

We also vary the boundaries of the unstable region in our next set of simulations, Cases 28–32, but we do so by moving the innermost radius of instability to 20 instead of 6. These would be expected to have steeper PSDs for outer boundaries of the same value (100, e.g. Cases 19–27), because the fastest moving zones at the smallest radii, which contribute more power at the highest frequencies, are no longer included. Case 28, with $i = 0^\circ$, is also expected to provide our results closest to the original results of Mineshige et al. (1994a), since we use the same outer radius, but a somewhat smaller inner radius and the difference between the Newtonian and pseudo-Newtonian potentials are $< 10\%$ when $r_N = 20$. Indeed, for all these simulations $\beta = 1.65 \pm 0.04$, in rather good agreement with the earlier non-relativistic work. The effect of varying the inclination angle is very small here, since the GR effects are weak. This relative lack of GR effects is because the closest emission now comes from $20r_g$; this implied we did not need to compute as many intermediate angle cases.

It is also instructive to compare these Cases 28–32 with the second set (10–18), in that the ratios of r_1/r_N are very similar (5 against 5.33). Our earlier work (WX) argued that the ratio of the outer to the inner edge of the unstable zone was a key determinant of the PSD slope, and indeed the slopes for $i = 0$ are not too dissimilar (1.55 vs. 1.68). Furthermore, the gravitational red-shift acting more strongly in Case 10 than in Case 28 could explain the bulk of that modest difference. But once the viewing angle departs significantly from face-on, the GR induced differences become quite substantial indeed, and we conclude that the ratio of inner to outer zone radii is not a dominating variable. Rather, what is most important is the breadth of the zone of instability, as long as the inner boundary thereof is not far from the marginally stable orbit.

Cases 33–37 illustrate the effects of different prescriptions for propagating the instability within the disk. The standard models of Mineshige et al. (1994a, b) utilized a rough prescription for differential rotation, whereby if the (i, j) zone went unstable, its dumped mass was equally transferred to the $(i + 1, j + 1 - I)$, $(i + 1, j + 2 - I)$ and $(i + 1, j + 3 - I)$ zones. They typically considered $I = 1$, as have we throughout the simulations so far; the value in the Rot. column of Table 1 is the value of I used in the simulations. Mineshige et al. (1994a) also considered a case where $I = 0$ and $I = 2$ and found little difference in results. No differential rotation, other than that enforced by the quasi-Keplerian azimuthal velocity (Eqn. 3), is modeled by $I = 0$, and we have considered this in Cases 33 and 36, which are the analogs to Cases 2 and 4 for $I = 1$. We find modest, and consistent deviations, with $\Delta\beta = 0.05$ for Case 33 vs. Case 2 ($i = 30^\circ$) and $\Delta\beta = 0.06$ for Case 36 vs. Case 4 ($i = 60^\circ$). When we consider larger amounts

of “differential rotation”, with $I = 3$ and $I = 5$, the results differ hardly at all from the “rigid rotation” case for lower inclination angle, but the deviations increase with I , up to a total of $\Delta\beta = 0.15$ between $I = 1$ and $I = 5$ for $i = 60^\circ$. While these changes are not that dramatic, we again find greater GR effects at higher viewing angles. Note that in all these cases the actual velocity field is Keplerian and the differences as to which zones are triggered do not directly affect the Doppler boosting calculations; however, different choices for I do determine which zones are included in the “avalanche” and therefore can modify the total energy released.

We also briefly considered what would happen if an unstable zone shared its dumped mass with zones not just inward of it, but also to its sides and outward. The rationale for doing so and the way in which we implemented this modification was discussed above, in §3.1. Only two such simulations were performed (Cases 38 and 39), and the column headed “Diff.” distinguishes them, in that the trigger is spread in all directions as opposed to just inward, as is the case for every other simulation. As was the situation when GR effects were ignored, we found a substantial steepening of the PSD, with $\Delta\beta = 0.28$ for $i = 30^\circ$ and $\Delta\beta = 0.43$ for $i = 60^\circ$. We can understand this result because such a spreading of the triggering would encourage more longer-lived flares concentrated at the outer portion of the disk, putting relatively more power in the lower frequency bins. We note that we did not extend the approach of Mineshige et al. (1994b; cf. §2.1) wherein slow accretion always occurred, independent of whether any zone was unstable in a given timestep, to include GR effects. Our non-relativistic simulations of this situation agreed well with theirs, and so we expect the modifications produced by GR as discussed above to act in concert with those produced by simulations including weak infall at a constant rate.

Our final set of simulations, Cases 40–43, examines the influence of the size of the trigger. Our earlier non-relativistic simulations had considered a substantial number of variations in the relative size of the trigger (the dumped mass, m_d) and the initial deviation from the critical mass in each zone. Those simulations (WX) found only very small changes in the PSDs produced after the simulations were run for long times, although early-time light curves could be very different. So we expected little dependence on m_d even when GR effects were included, and this turns out to be so. While we chose $m_d = 2$ for all other cases, here we considered an order of magnitude range, $m_d = [0.5, 5.0]$. The total range in the PSD slope was only 0.07 for $i = 30^\circ$ and 0.09 for $i = 60^\circ$; in both cases the larger dumped masses ($m_d = 5.0$) produce steeper power spectra, while the smaller triggers ($m_d = 0.5$) yield shallower slopes.

As is clear from Figs. 2–4, in many cases the PSD is not perfectly described as a single power-law, even over

the limited region in which we calculate our β values. The lowest frequencies, where the PSD rises, must clearly be excluded in a computation of an approximate power-law. The highest frequencies plotted exclude a unphysical turnaround and thereby correspond to a cut-off below the Nyquist limit. The slight hump in the PSD (around $f = 100$) is more pronounced at higher inclination angles (cf. Fig. 4), and is clearly induced by GR effects. Oscillations in the PSD at high frequencies are also sometimes observed (e.g. Figs. 2 and 4), perhaps indicating a sort of QPO behavior at the highest frequencies, though the overall slope is only negligibly affected by these deviations from a simple power-law.

5. Conclusions

Our extension of attempts to produce SOC situations on accretion disks around BHs by including GR effects have shown substantial variations in detailed light curves and in the power spectrum of the fluctuations. Strong dependences on viewing angle are noted and the details thereof differ from the preliminary estimates by Abramowicz and Bao (1994), particularly at lines-of-sight very close to the disk (though we note that in reality, such extreme viewing angles are unlikely, as they could be obscured by the wider outer regions of the disks, or, in the case of AGN, surrounding tori). Dramatic differences in the slope of the PSD are found when different inner and outer radii for the unstable disk region are considered. This critical result is independent of viewing angle and propagation effects, as can be seen from Table 1 for Cases 1, 10, 19 and 28. The PSD slope actually becomes flatter than is ever observed if the outer radius of the unstable zone is too large ($\sim 100r_g$ for the inner edge fixed at the marginally stable orbit). Unsurprisingly, GR effects become unimportant if the inner boundary of the unstable region ends at radii substantially greater than $6GM/c^2$. Very large changes in the PSDs are also engendered by different assumptions about how the triggering spreads through the disk. Nonetheless, several other parameters induce only minor changes in the long-term light curves and power spectra: modifications in the nominal rotation prescription; changes to the mass dumped from an unstable zone; and the size of the initial deviations from the critical state.

Given these many variations, it is only fair to conclude that self-organized criticality, in its *strictest sense*, is *not* produced, even in these highly idealized accretion disk models. The fundamental reason for this is that the basic units of energy release are no longer the same; rather, the amount of energy released deeper in the gravitational well is more substantial for a given mass traversing a given distance. (This effect is independent of whether uniform or logarithmically spaced radial zones are used in the computations.) When GR effects are included, the scale-free

nature required of an SOC process is further disrupted; the existence of a physical scale (r_g) in the potential breaks a fundamental symmetry really necessary for a complete SOC situation to be realized. Variations in the slope of the PSD can be understood by considering which portions of the disk release relatively more energy and by how the observations are affected by Doppler shifts, light bending and focusing. In addition, we saw that non-power law features can be imposed on the observed PSDs with the proper inclusion of GR effects.

Although a more realistic physical model might modify the statement concerning concentrated energy release made in the previous paragraph, it probably would not do so. For example, consider magnetic flares based on reconnection events, the basic physical background, explicit in the models of Lu & Hamilton (1991) and indirectly invoked by Mineshige et al. (1994a): if the energy density in the magnetic fields is close to equipartition with the pressure in the matter, then higher energy releases would still be expected closer to the inner edge of the disk. (In the case of solar flares explicitly considered by Lu & Hamilton, the assumption that the reconnection process is nearly scale-free is more nearly viable than in the case of accretion disks.) Therefore, even when the disk is operating right at the “hairy edge” of stability, so that flares of many different sizes can indeed be randomly triggered by a single infalling mass unit (or reconnection event) at the outer edge of the unstable portion of the disk, thus implying that an *approximate* SOC state exists, we do not see all the properties of a full self-organized criticality. This is true even when the variations induced by GR on the propagation of the emitted photons are ignored. We stress that the key observables, i.e., the light curves and PSD, still depend on the size and location of the region over which the instability operates; therefore, they are *not completely independent of boundary conditions*, or other small details, as would be the case for a system that is in a *full-fledged* SOC state.

Finally, GR effects certainly make significant differences in what is observed, although, since they involve the propagation of photons after leaving the disk, those externally produced changes should not additionally count against a claim that SOC has been established. Nonetheless, it is intriguing that these models typically reproduce variability power spectrum slopes between -1.0 and -2.0 , as this also seems to span the range of observed PSD slopes seen in both galactic and extragalactic variable sources. Therefore, the importance of quasi-SOC situations remains an intriguing possibility, and more careful physical models for the triggering of flares of a variety of strengths within and above accretion disks are well worth studying.

We thank the anonymous referee for suggesting several important corrections and clarifications. PJW is most

grateful for hospitality at the Department of Astrophysical Sciences of Princeton University where the writing of this paper was completed. This work was supported by NASA Grant NAG 5-3098 and by Research Program Enhancement funds at Georgia State University.

References

- Abramowicz, M.A., Bao, G. 1994, PASJ 46, 523
- Abramowicz, M.A., Bao, G., Lanza, A., Zhang, X.-H. 1989, in Proc. 23rd ESLAB Symp. on Two Topics in X-Ray Astronomy ed J. Hunt, B. Battick. ESA Sp-296, (European Space Agency), p871
- Abramowicz, M.A., Bao, G., Lanza, A., Zhang, X.-H. 1991, A&A 245, 454
- Abramowicz, M.A., Bao, G., Larsson, S., Wiita, P.J. 1997, ApJ 489, 819
- Abramowicz, M.A., Lanza, A., Spiegel, E.A., Szuszkiewicz, E. 1992, Nature 356, 41
- Artimova, I.V., Björnsson, G., Novikov, I.D. 1996, ApJ 461, 565
- Bak, P., Tang, C., Wiesenfeld, K. 1987, Phys. Rev. Lett. 59, 381
- Bak, P., Tang, C., Wiesenfeld, K. 1988, Phys. Rev. A. 38, 364
- Bao, G., Abramowicz, M.A. 1996, ApJ 465, 646
- Bao, G., Hadrava, P., Ostgaard, E. 1994, ApJ 435, 55
- Bao, G., Hadrava, P., Wiita, P.J., Xiong, Y. 1997, ApJ 487, 142
- Bao, G., Wiita, P.J. 1997, ApJ 485, 136
- Bao, G., Wiita, P.J. 1999, ApJ 519, 80
- Bao, G., Wiita, P.J., Hadrava, P. 1996, Phys. Rev. Lett. 77, 12
- Bao, G., Wiita, P.J., Hadrava, P. 1998, ApJ, 504, 58
- Bracco, A., Provenzale, A., Spiegel, E.A., Yecko, P. 1999, in Theory of Black Hole Accretion Disks, ed M.A. Abramowicz, G. Björnsson, J.E. Pringle, (Cambridge University Press, Cambridge) p274
- Chakrabarti, S.K. 1996, Phys. Reports 266, 229
- Chakrabarti, S.K., Wiita, P.J. 1993, ApJ, 411, 602
- Chen, X., Abramowicz, M.A., Lasota, J.-P., Narayan, R., Yi, I. 1995, ApJ 443, L61
- Dennis, B.R. 1985, Solar Physics 100, 465
- Ichimaru, S. 1977, ApJ, 214, 840
- Lawrence, A., Papadakis, I. 1993, ApJ 414, L85
- Lightman, A.P., Eardley, D.M. 1974, ApJ 187, L1
- Lu, E.T. 1995, ApJ 446, L109
- Lu, E.T., Hamilton, R.J. 1991, ApJ 380, L89
- Mangalam, A.V., Wiita, P.J. 1993, ApJ 406, 420
- Manmoto, T., Takeuchi, M., Mineshige, S., Matsumoto, R., Negoro, H. 1996, ApJ 464, L135

- Mineshige, S., Negoro, H. 1999, in High Energy Processes in Accreting Black Holes, ASP Conf. Ser. 161, ed. J. Poutonen, R. Svensson (Astr. Soc. Pacific, San Francisco) p113
- Mineshige, S., Ouchi, N.B., Nishimori, H. 1994a, PASJ 46, 97
- Mineshige, S., Takeuchi, M., Nishimori, H. 1994b, ApJ 435, L125
- Miyamoto, S., Iga, S., Kitamoto, S., Kamado, Y. 1993, ApJ 403, L39
- O'Brien, K., Wu, L., Nagel, S.R. 1991, Phys. Rev. A 43, 2052
- Paczynski, B., Wiita, P.J. 1980, A&A, 88, 23
- Parker, E.N. 1988, ApJ, 330, 474
- Press, W.H. 1978, Comments Ap. 7, 103
- Sawada, K., Matsuda, T., Hachisu, I. 1986, MNRAS 221, 679
- Shakura, N.I., Sunyaev, R.A. 1973, A&A 24, 337
- Stern, B.E., Svensson, R. 1996, ApJ 469, L109
- Takeuchi, M., Mineshige, S. 1997 ApJ, 486, 160
- Takeuchi, M., Mineshige, S., Negoro, H. 1995, PASJ 47, 617
- Vaughn, B.A., Nowak, M.A. 1997, ApJ 474, L43
- Wiita, P.J., Miller, H.R., Carini, M.T., Rosen, A. 1991, in Structure and Emission Properties of Accretion Disks, ed C. Bertout, S. Collin-Souffrin, J.P. Lasota, J. Tran Thanh Van, 6th I.A.P. Astrophysics Meeting / I.A.U. Colloq. 129, (Editions Frontières, Gif-sur-Yvette) p557
- Wiita, P.J., Xiong, Y. 1999, in Theory of Black Hole Accretion Disks, ed M.A. Abramowicz, G. Björnsson, J.E. Pringle, (Cambridge University Press, Cambridge) p274 (WX).
- Yonehara, A., Mineshige, S., Welsh, W.F. 1997, ApJ 486, 388
- Zhang, X.-H., Bao, G. 1991, A&A 246, 21

Table 1. Parameters and Results of Selected Simulations.

Case	r_{in}	r_{out}	i	Rot.	Diff.	m_d	β
1	6	19	0	1	in	2	1.69
2	6	19	30	1	in	2	1.55
3	6	19	45	1	in	2	1.43
4	6	19	60	1	in	2	1.35
5	6	19	65	1	in	2	1.35
6	6	19	70	1	in	2	1.34
7	6	19	74	1	in	2	1.36
8	6	19	80	1	in	2	1.43
9	6	19	85	1	in	2	1.56
10	6	32	0	1	in	2	1.55
11	6	32	30	1	in	2	1.38
12	6	32	45	1	in	2	1.33
13	6	32	60	1	in	2	1.33
14	6	32	65	1	in	2	1.23
15	6	32	70	1	in	2	1.20
16	6	32	74	1	in	2	1.21
17	6	32	80	1	in	2	1.26
18	6	32	85	1	in	2	1.30
19	6	100	0	1	in	2	1.02
20	6	100	30	1	in	2	0.93
21	6	100	45	1	in	2	0.86
22	6	100	60	1	in	2	0.83
23	6	100	65	1	in	2	0.79

Table 1, continued. Parameters and Results of Selected Simulations.

24	6	100	70	1	in	2	0.79
25	6	100	74	1	in	2	0.76
26	6	100	80	1	in	2	0.75
27	6	100	85	1	in	2	0.77
28	20	100	0	1	in	2	1.68
29	20	100	30	1	in	2	1.69
30	20	100	60	1	in	2	1.69
31	20	100	70	1	in	2	1.64
32	20	100	85	1	in	2	1.62
33	6	19	30	0	in	2	1.60
34	6	19	30	3	in	2	1.59
35	6	19	30	5	in	2	1.59
36	6	19	60	0	in	2	1.41
36	6	19	60	3	in	2	1.46
37	6	19	60	5	in	2	1.51
38	6	19	30	1	all	2	1.83
39	6	19	60	1	all	2	1.78
40	6	19	30	1	in	0.5	1.58
41	6	19	30	1	in	5	1.51
42	6	19	60	1	in	0.5	1.43
43	6	19	60	1	in	5	1.34

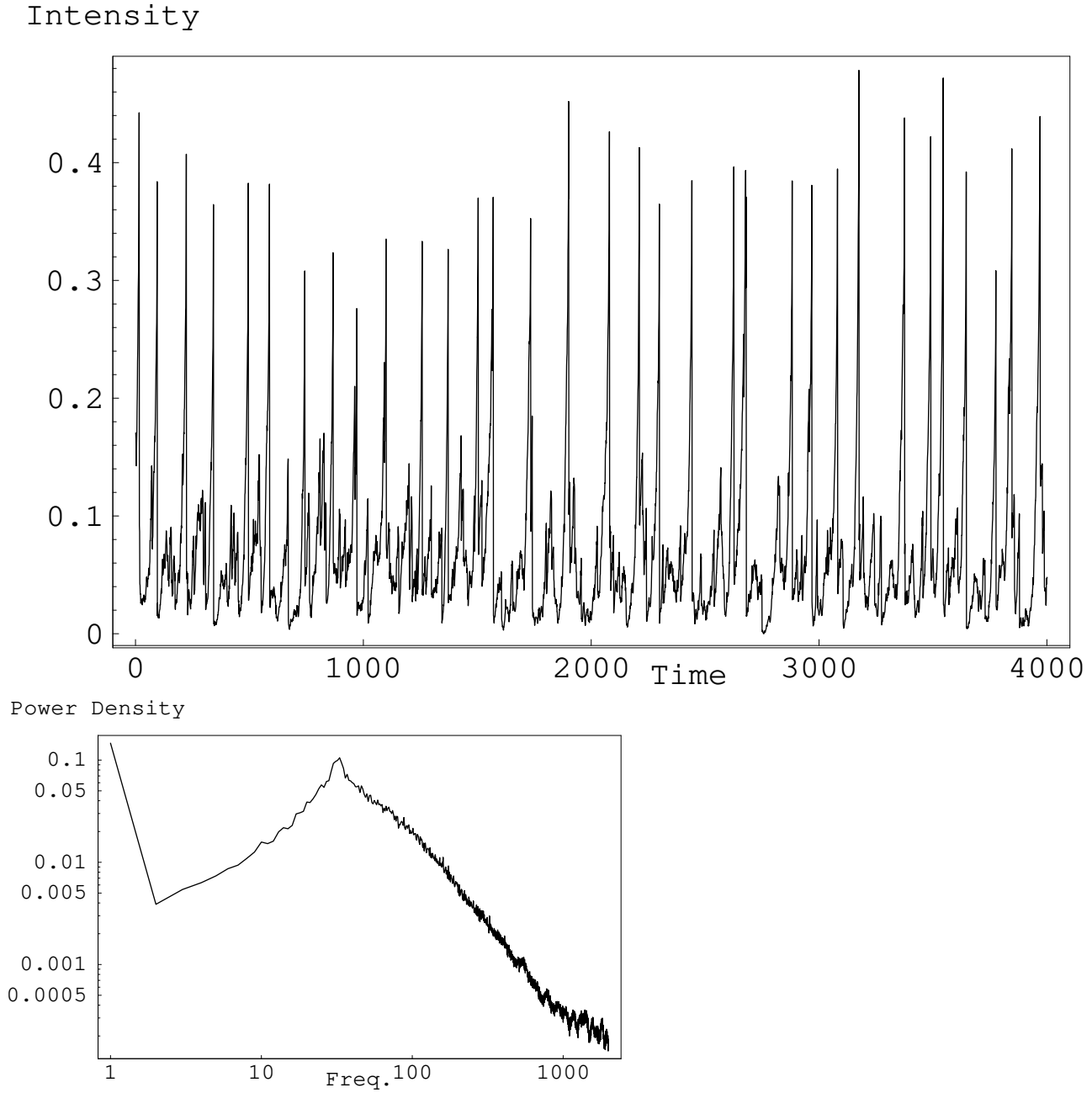


Fig. 1.. (a) A portion of the light curve for Case 2, with $r_{in} = 6, r_{out} = 19, i = 30^\circ$. This segment is chosen to be short enough to allow fine structure to be seen and is also selected from a piece of the entire simulation far enough developed so that any initial condition effects have dissipated. (b) The power spectrum density for Case 2; this curve is a mean of PSDs computed from eight equal segments of the light-curve, and the value of its slope, β , quoted in Table 1, is fit to this curve to frequencies between 50 and 2048.

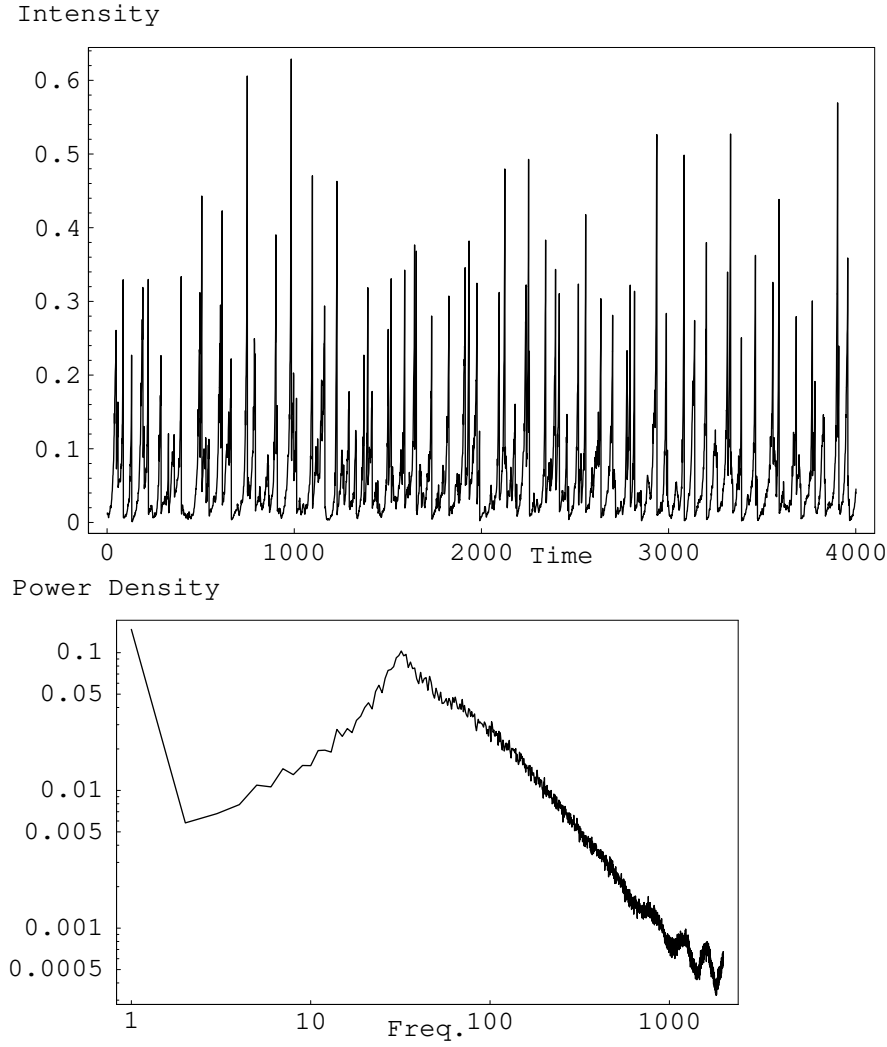


Fig. 2.. As in Fig. 1 for Case 11, with $r_{in} = 6, r_{out} = 32, i = 30^\circ$. Note that these figures all have different y-axis scales.

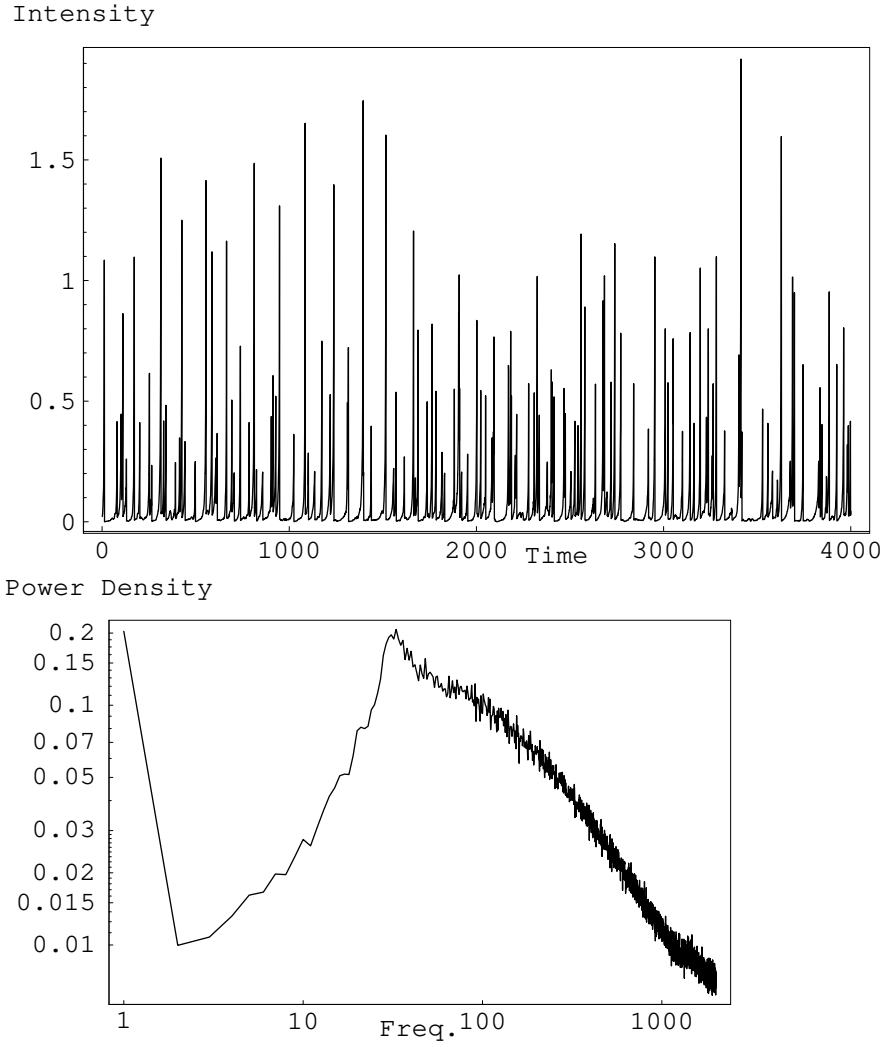


Fig. 3.. As in Fig. 1 for Case 20, with $r_{in} = 6, r_{out} = 100; i = 30^\circ$.

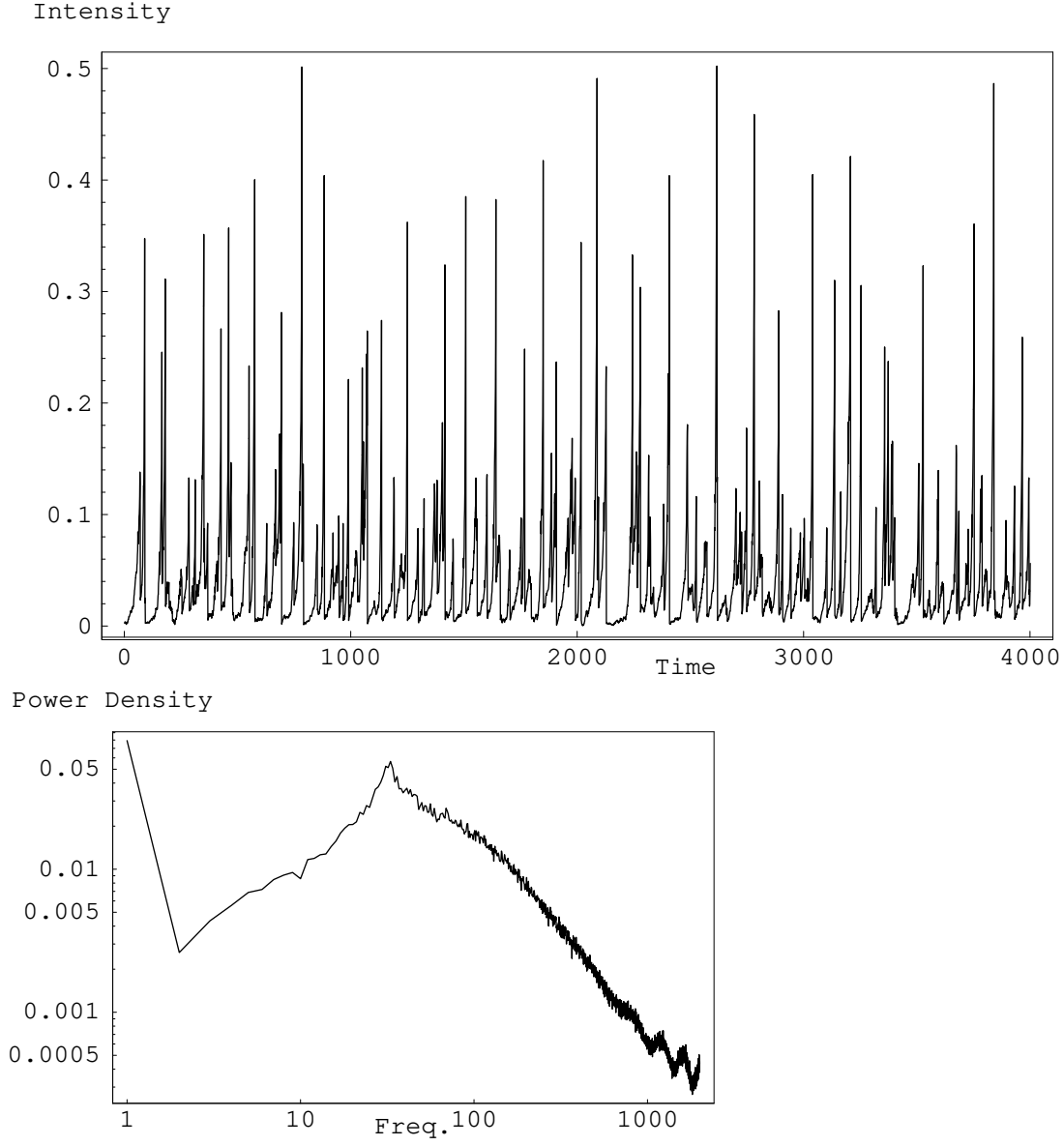


Fig. 4.. As in Fig. 1 for Case 13, with $r_{in} = 6$, $r_{out} = 32$, $i = 60^\circ$.